The Astrophysical Journal, 889:60 (12pp), 2020 January 20 https://doi.org/10.3847/1538-4357/ab5b96

Cosmological Simulation of Galaxy Groups and Clusters. I. Global Effect of Feedback from Active Galactic Nuclei

Rudrani Kar Chowdhury[1], Suchetana Chatterjee[1], Anto. I. Lonappan[1,2,3], Nishikanta Khandai[4], and Tiziana Di Matteo[5]
[1] Department of Physics, Presidency University, Kolkata, 700073, India
[2] Astrophysics and Cosmology, Scuola Internazionale Superiore di Studi Avanzati, via Bonomea, I-265-34136 Trieste, Italy
[3] Institute for Fundamental Physics of the Universe (IFPU), Via Beirut 2, I-34014 Trieste, Italy
[4] School of Physical Sciences, National Institute of Science Education and Research, HBNI, Jatni–752050, India
[5] McWilliams Center for Cosmology, Carnegie Mellon University, Pittsburgh, PA 15213, USA
Received 2019 July 11; revised 2019 November 16; accepted 2019 November 18; published 2020 January 24

Abstract

In this study we quantify the properties of the gas and dark matter around active galactic nuclei (AGNs) in simulated galaxy groups and clusters and analyze the effect of AGN feedback on the surrounding intracluster (group) medium. Our results suggest downsizing of AGN luminosity with host halo mass, supporting the results obtained from clustering studies of AGNs. By examining the temperature and density distribution of the gas in the vicinity of AGNs we show that due to feedback from the central engine, the gas gets displaced from the center of the group/cluster resulting in a reduction of the density but an enhancement of temperature. We show that these effects are pronounced at both high and low redshifts and propose new observables to study the effect of feedback in higher-redshift galaxies. We also show that the average stellar mass is decreased in halos in the presence of AGN feedback confirming claims from previous studies. Our work for the first time uses a fully cosmological hydrodynamic simulation to evaluate the global effects of AGN feedback on their host dark matter halos as well as galaxies at scales of galaxy groups and clusters.

Unified Astronomy Thesaurus concepts: Galaxy clusters (584); Active galactic nuclei (16)

1. Introduction

It is currently believed that every massive galaxy in the universe harbors a central supermassive black hole (SMBH) of mass ranging between 10^6–$10^9 M_\odot$ (e.g., Soltan 1982; Ferrarese & Merritt 2000; Merritt & Ferrarese 2001; Gültekin et al. 2009). Some of them have active accretion disks and they grow by accreting gas from their surroundings. These classes of SMBH are known as active galactic nuclei (AGNs). As they grow by accreting matter from their neighboring environments they release a large amount of energy into their surroundings. Some fraction of the radiated energy couples to the surrounding gas in a process known as AGN feedback (e.g., Silk & Rees 1998; Ciotti & Ostriker 2001; Nath & Roychowdhury 2002; Kaiser & Binney 2003; Nulsen et al. 2004; Di Matteo et al. 2005; Springel et al. 2005; Cox et al. 2006; Raychaudhury et al. 2009; Chaudhuri et al. 2013; Chatterjee et al. 2015; Costa et al. 2015; Harrison et al. 2018; Penny et al. 2018).

Many studies show that AGN feedback has observable effects on galaxy formation known as AGN–galaxy coevolution in the literature (e.g., Kauffmann & Haehnelt 2000; Wyithe & Loeb 2003; Marconi et al. 2004; Shankar et al. 2004; Cattaneo et al. 2006; Croton et al. 2006; Hopkins et al. 2006b; Lapi et al. 2006, 2014; Di Matteo et al. 2008; Booth & Schaye 2009; Volonteri et al. 2011; Conroy & White 2013; Caplar et al. 2015; Oogi et al. 2016; Lanzuisi et al. 2017; Mutlu-Pakdil et al. 2018). Several properties of the host galaxy or the surrounding environment of the central engine are linked with the central SMBH itself. For example, there exists strong correlation between the central black hole mass and the stellar velocity dispersion (e.g., Ferrarese & Merritt 2000; Tremaine et al. 2002; Ferrarese & Ford 2005). Also, other properties of the galaxy such as bulge luminosity (e.g., Dressler 1989; Kormendy & Richstone 1995; Marconi & Hunt 2003; Graham 2007), bulge mass (e.g., Magorrian et al. 1998; Häring & Rix 2004), Sérsic index (e.g., Graham & Driver 2007), kinetic energy of the random motion of the bulge (e.g., Feoli & Mancini 2009), gravitational binding energy (e.g., Aller & Richstone 2007), virial mass of the galaxy (e.g., Ferrarese et al. 2006) are tightly coupled to the mass of the central SMBH. Studies show that the effective radius of galaxies is correlated with the residual of $M_{\rm BH}$–σ and $M_{\rm BH}$–$L_{\rm Bulge}$ relations (e.g., Marconi & Hunt 2003; Hopkins et al. 2007a, 2007b). It has been also suggested that there exists a plane of correlation between black hole mass, galaxy size, and bulge mass, known as the black hole fundamental plane (e.g., Hopkins et al. 2007b; Beifiori et al. 2012; Saikia et al. 2015; van den Bosch 2016).

Other observable effects of AGN feedback include the $L_{\rm X}$–T relation in galaxy groups and clusters (e.g., Arnaud & Evrard 1999; Nath & Roychowdhury 2002; Scannapieco & Oh 2004; Lapi et al. 2005; Peterson & Fabian 2006; Thacker et al. 2009; Puchwein et al. 2010; Bharadwaj et al. 2015; Voit et al. 2018), Sunyaev–Zeldovich (SZ: Sunyaev & Zeldovich 1972) effect (e.g., Bhattacharya et al. 2008; Chatterjee et al. 2008, 2010; Ruan et al. 2015; Crichton et al. 2016; Spacek et al. 2016; Verdier et al. 2016; Lacy et al. 2019), SZ power spectrum (Chatterjee & Kosowsky 2007; Scannapieco et al. 2008; Battaglia et al. 2010), reduced star formation rate (e.g., Kauffmann et al. 2003; Vitale et al. 2013; Vaddi et al. 2016; Kakkad et al. 2017; Terrazas et al. 2017), which have been addressed in the literature.

Theoretical models of this paradigm of coevolution has been explored by numerous groups (e.g., Granato et al. 2004; Vittorini et al. 2005; Hopkins et al. 2006a; Monaco et al. 2007; Pelupessy et al. 2007; Johansson et al. 2009; Aversa et al. 2015; Li et al. 2015; Lu & Mo 2015; Biernacki et al. 2017). All of these models explain the observed correlation in terms of strong feedback from the AGN (Silk & Rees 1998; Di Matteo et al. 2005; Cox et al. 2006; McCarthy et al. 2010; Heckman & Best 2014; Choi et al. 2015; Steinborn et al. 2015; Baron et al. 2017; Yang et al. 2018).

Theoretical studies have been undertaken to explain the effect of AGN feedback on the surrounding hot gas in galaxy groups and clusters (e.g., Hambrick et al. 2011; Gaspari et al. 2012; Choi et al. 2015). To study the effect of AGN feedback on large-scale structure and to evaluate its importance for the evolutionary history of the universe, AGN feedback has been introduced in cosmological simulations (e.g., Zanni et al. 2005; Pelupessy et al. 2007; Sijacki et al. 2007, 2015; Bhattacharya et al. 2008; Chatterjee et al. 2008; Di Matteo et al. 2008; Johansson et al. 2009; McCarthy et al. 2010; Genel et al. 2014; Hirschmann et al. 2014; Vogelsberger et al. 2014a, 2014b; Li et al. 2015; Nelson et al. 2015; Steinborn et al. 2015; Schaye et al. 2015; Liu et al. 2016; Beckmann et al. 2017; Biernacki et al. 2017; Scholtz et al. 2018; Peirani et al. 2019).

Recently, Khandai et al. (2015) ran a cosmological simulation MassiveBlack- II to study a large representative volume of the universe with a spatial resolution of ∼*few* kpc. Using this simulation we study the effect of AGN feedback on its surrounding medium by evaluating the correlation between AGN activity with the properties of the intracluster medium (ICM) as well as the host dark matter halos of AGN. The paper is structured as follows. In Section 2, we briefly discuss the simulation and the data used for our work. In Section 3, we present the results. In Section 4, we discuss and summarize our results.

2. Simulation

The simulation for this work uses an extended version of the parallel cosmological Tree Particle Mesh-Smoothed Particle Hydrodynamics code GADGET2 (Springel 2005) and an upgraded version of it (GADGET3). Both simulations are based on the Lambda cold dark matter (ΛCDM) cosmology with cosmological parameters adopted from Spergel et al. (2003) and Komatsu et al. (2011), respectively. We note that the different cosmological parameters will not affect the results of this paper. We refer the reader to Li et al. (2007) and Sijacki et al. (2007) for a detailed discussion in this regard. In this work we use two versions of the simulations namely: by Di Matteo et al. (2008) (D08 hereafter) and Khandai et al. (2015; K15 hereafter). D08 uses a simulation box of size 33.75 Mpc, while the box size is much bigger for K15 (100 Mpc).

Both simulations have dark matter and gas dynamics. The simulations also include radiative gas cooling, star formation, black hole growth, and feedback. The gas dynamics is modeled using the Lagrangian smoothed particle hydrodynamics (SPH) technique (Monaghan 1992) and radiative cooling and heating processes are modeled using the prescription of Katz et al. (1996). As these are cosmological volume simulations, the spatial resolution limits us probing physical scales of star formation or black hole accretion. Hence, to model these processes approximation schemes have been introduced. Star formation and supernova feedback are implemented in the simulation through a sub-resolution multiphase model developed by Springel & Hernquist (2003).

Black hole accretion and feedback is modeled according to the prescription of Di Matteo et al. (2008) and Di Matteo et al. (2005). Black holes are assumed to be collisionless sink particles that can grow by accreting matter from the intervening medium or through galaxy mergers. The Bondi–Hoyle spherical accretion relation (Bondi & Hoyle 1944; Bondi 1952) is used to quantify the accretion rate of the black hole. The accretion rate of gas onto the black hole is given by

$$\dot{M}_{\rm BH} = 4\pi \frac{(G^2 M_{\rm BH}^2 \rho)}{(c_s^2 + v^2)^{\frac{3}{2}}}, \quad (1)$$

where ρ and c_s are the density and speed of sound of the surrounding gas, respectively, v is the velocity of the black hole relative to the surrounding gas and G is the universal gravitational constant. We note that due to limited resolution, the physical parameters in the Bondi–Hoyle relation are adopted from larger scales and adjusted with an appropriate boost factor (Di Matteo et al. 2005, 2008; Springel et al. 2005; Pelupessy et al. 2007).

The bolometric radiation coming out of the black hole is given by $L_{\rm bol} = \eta \dot{M}_{\rm BH} c^2$, where η is the canonical efficiency and its value is taken to be 0.1 for a radiatively efficient thin disk accretion (Shakura & Sunyaev 1973). A part of this radiated energy gets associated with the local gas and is deposited on every gas particle according to a kernel function, as feedback energy $E_{\rm f}$ such that $\dot{E}_{\rm f} = \varepsilon_{\rm f} L_{\rm bol}$ (Di Matteo et al. 2008). ε_f is the feedback efficiency and its value is chosen to be 0.05 to match the normalization of $M_{\rm BH}$–σ relation with the current observation (Di Matteo et al. 2005). For simplicity it is assumed that feedback energy is coupled to the surrounding medium isotropically. Mechanical energy coming out of the AGN in the form of a jet can be anisotropic which is not modeled in the simulation. However, mechanical feedback has been explored by various other groups in cosmological simulations (Teyssier 2002; Cattaneo & Teyssier 2007; Teyssier et al. 2011; Vazza et al. 2013; Barai et al. 2014; Cielo et al. 2018).

The initial mass function of seed SMBH is unknown and hence to address the initial mass function the following prescription is adopted. The simulation runs an in situ halo-finder algorithm and populates a halo with a seed SMBH when the mass of the halo exceeds a certain threshold. Halos are identified in this simulation with a friends-of-friends algorithm (Davis et al. 1985). In this algorithm particles are linked together if they are within a certain distance (linking length b), which is taken in K15 as $0.2\bar{l}$ ($\bar{l}$ being the mean particle separation). All the dark matter particles within this distance are taken altogether to form a halo. By this, all other particles, such as gas, stars, and BHs also fall within the potential of their nearest DM halo. For identifying substructures within the halos the SUBFIND algorithm is used (Springel et al. 2001). A seed black hole of mass $\approx 10^5 h^{-1} M_\odot$ is created within a halo of mass $\approx 10^{10} h^{-1} M_\odot$ if the halo does not contain any black hole. The seed black hole is now allowed to grow through gas accretion and merger events.

We use the K15 data for two redshifts ($z = 1.0$ and $z = 0.1$) to study the redshift evolution of the central AGNs and their host galaxies as a result of feedback on them. The K15 simulation was evolved up to $z = 0$ but to compare our results with the D08 data we used the $z = 1$ snapshot of K15. The larger box size of K15 comes with the following advantages that are crucial to our work: the number of higher-mass halos and higher-luminosity AGNs increases with box size. These increases in number provide adequate statistics to probe the high end of the AGN luminosity as well as its host halo mass function. We discuss this issue further later. The simulation parameters for both the simulations are listed in Table 1, where N_p is the total number of gas + dark matter (DM) particles in

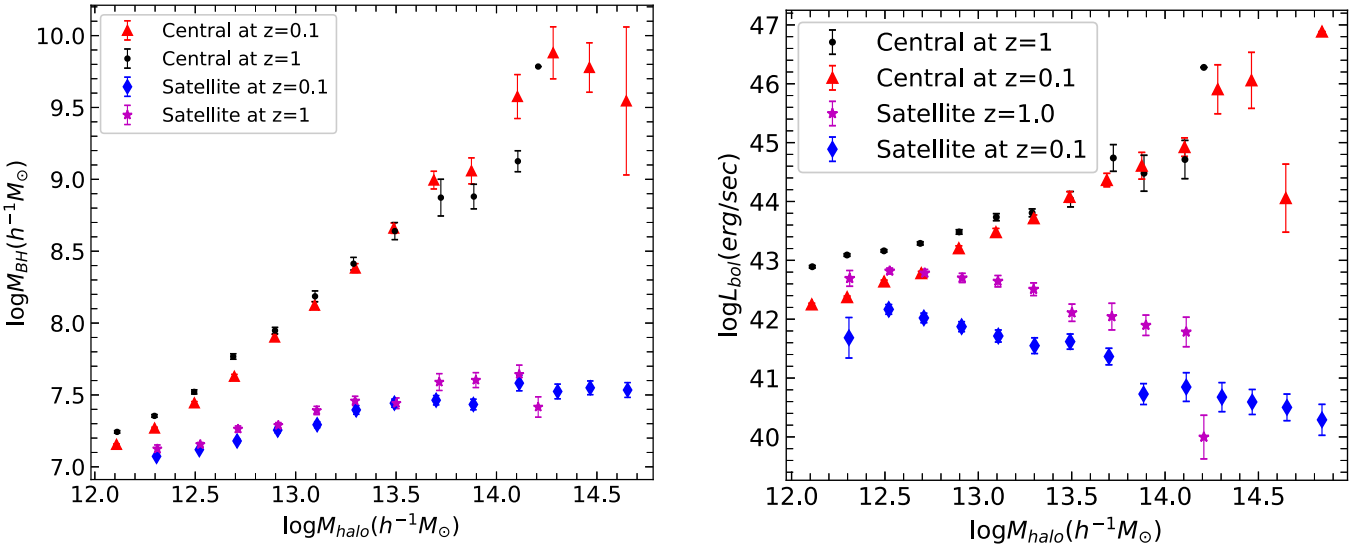

Figure 1. Left panel : $M_{\rm halo}$–$M_{\rm BH}$ relation in the K15 simulation at $z = 1$ and at $z = 0.1$. The black dots and magenta stars show the central and satellite black holes, respectively at $z = 1$, while the red triangles and blue diamonds represent the central and satellite black holes, respectively, at $z = 0.1$. We do not see any redshift dependence for these correlations. Central BH mass increases steeply with their host halo mass, while the satellite BH mass increases very slightly with the halo mass and then gets saturated at the higher host halo mass range. Right panel : $M_{\rm halo}$–$L_{\rm bol}$ relation in the K15 simulation at $z = 1$ and $z = 0.1$. The color scheme is the same as the left panel. Clearly, the luminosities of the satellite black holes decrease in the higher halo mass bins for both redshifts. We propose that this downsizing effect is due to AGN feedback. See Sections 3 and 4 for more details.

Table 1
The Parameters of the D08 and K15 Simulations

Simulation	Box size (h^{-1} Mpc)	N_p	$m_{\rm DM}$ ($h^{-1}M_\odot$)	$m_{\rm gas}$ ($h^{-1}M_\odot$)	ε (h^{-1}kpc)	$z_{\rm end}$
D08	33.75	2×216^3	2.75×10^8	4.24×10^7	6.25	1.0
K15	100	2×1792^3	1.1×10^7	2.2×10^6	1.85	0.0

Note. N_p, $m_{\rm DM}$, $m_{\rm gas}$, ε, $z_{\rm end}$ represent the total number of particles (dark matter+gas), mass of dark matter particles, initial mass of gas particles, gravitational softening length, and the final redshift, respectively.

the box, $m_{\rm DM}$ and $m_{\rm gas}$ are the mass resolutions for DM and gas particles respectively, ε is the gravitational softening length, and $z_{\rm end}$ is the final redshift up to which the simulation evolves. It is to be noted that without feedback cases are for the D4 simulation of Di Matteo et al. (2008), which has a different resolution than the Khandai et al. (2015) simulation. We note that the D6 simulation of Di Matteo et al. (2008) includes feedback and has a similar resolution to that of Khandai et al. (2015), although the box size of Khandai et al. (2015) is bigger. Chatterjee et al. (2008) did a resolution study between the D4 and D6 simulations. It was deduced from that study that resolution effects should not affect the overall conclusion but the details of the temperature and density maps might be different for different resolutions (as has been seen with the case of Sunyaev–Zeldovich fluxes in Chatterjee et al. 2008). Unless specified, our "with feedback" simulations are for K15 and "without feedback" simulations are for D4-D08.

For the current study we select black holes that have mass $\geqslant 10^7 h^{-1} M_\odot$. As already discussed, the simulation inserts seed BHs of mass $10^5 h^{-1} M_\odot$ when halos have a mass greater than $10^{10} h^{-1} M_\odot$. These black holes then grow by accretion or merger. We thus prefer to limit our analysis of black holes with mass well above the seed black hole mass to minimize the numerical noise. As a result of this, host halos of the lower-mass black holes are automatically being discarded. Thus, we are left with 2730 and 3702 black holes at $z = 1$ and $z = 0.1$, respectively. One of the goals of this study is to understand the role of AGNs on structure formation and hence a BH mass cutoff comes as a better choice since to first order, luminosity also scales as black hole mass. Also, it is seen that $M_{\rm BH}$ and $M_{\rm halo}$ are correlated but the onset of physical processes like AGN feedback alter these correlations and they can be studied in an unbiased way if we go to a mass limit away from the seed black hole mass. We checked that the effect of AGN feedback is evident at the higher end of both the halo mass and the black hole mass functions and hence the lower cutoff on black hole mass or halo mass will not alter our results.

In our work we study the scaling relations between the properties of the SMBH and their host halos. We also investigate the redshift evolution of those scaling relations. We propose the effect of AGN feedback on its surrounding medium to explain these scaling relations and a probe to study the interaction of the SMBH with its environment. To do this we focus on the diffuse gas as well as total stellar mass inside the halos. Density and temperature distributions of gas surrounding the AGN clearly reveal the effect of AGN feedback on its surrounding environment. We present these results in the following section.

3. Results

Figure 1 shows the correlation between the properties of the central BH with their host halos at $z = 1$ and $z = 0.1$ for K15. The BH population has been categorized into central and satellite BHs at both redshifts and the correlations of their

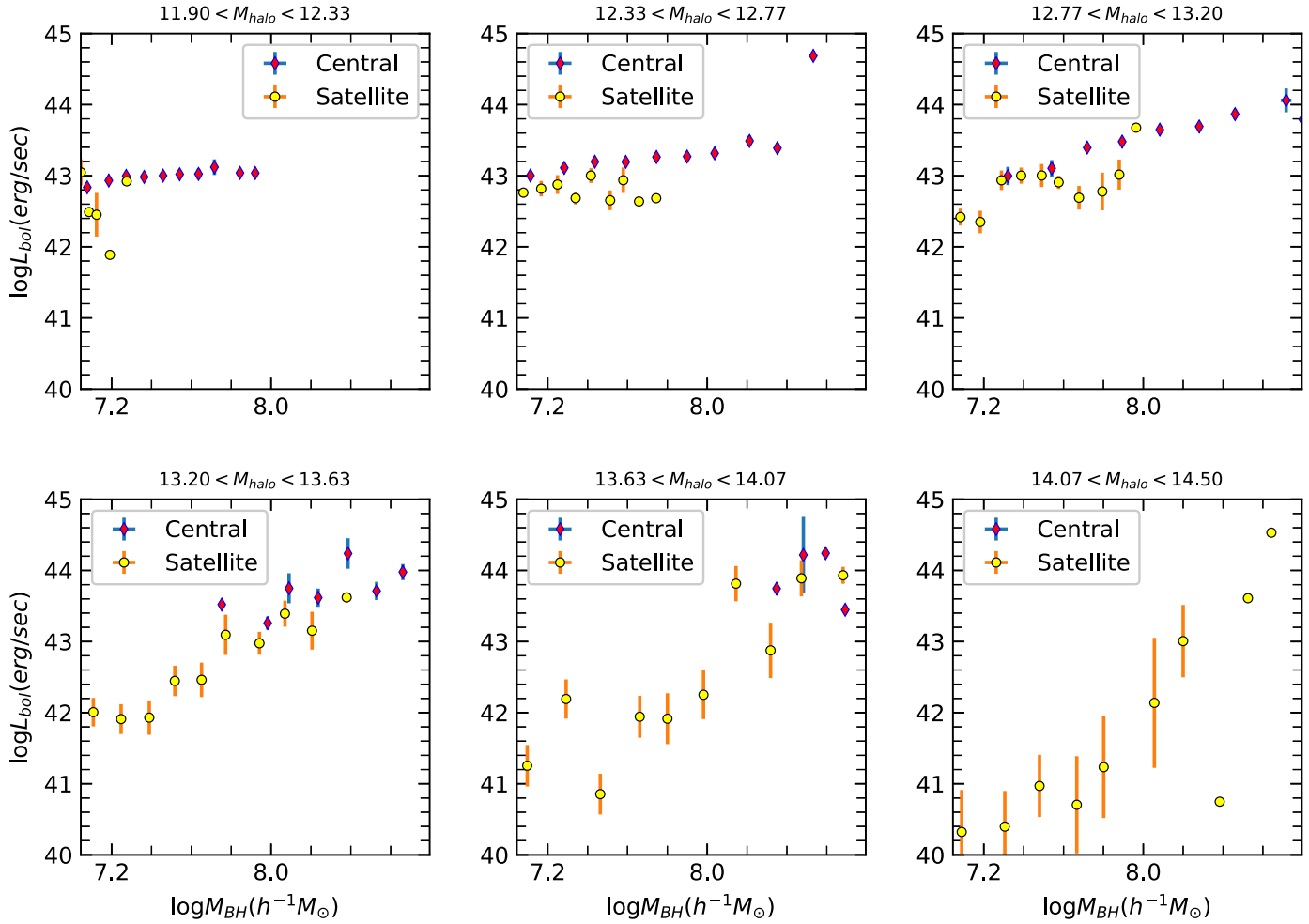

Figure 2. Conditional probability distribution of the $M_{\rm BH}$–$L_{\rm bol}$ correlations in the simulation at $z = 1$. The blue diamonds and yellow circles show the central and satellite black holes, respectively. The central AGN luminosity remains fairly constant with $M_{\rm BH}$ in the first two halo mass bins, then increases slightly at the higher halo mass scales. However, up to a mass scale of $\approx 10^{13.2} h^{-1} M_{\odot}$, the luminosity of the satellite AGN remains fairly constant. Above this mass scale there is a spread in the distribution of satellite AGN luminosities, and the luminosities are typically low at the highest-mass bin. The results are discussed in Sections 3 and 4.

masses with their host halo masses are shown in the left panel. The numbers of central BHs at $z = 1$ and $z = 0.1$ are 1956 and 2514, respectively, while the numbers of satellite BHs are 774 and 1188, respectively. It is observed that the central BH mass is increasing with host halo mass at both $z = 1$ and $z = 0.1$ and we do not see any significant redshift evolution of this correlation. The satellite BH mass slightly increases and then gets saturated at the higher-mass end of the host halos. The individual history of the most massive SMBH is discussed in Section 8 in K15. They have found that gas accretion dominates the growth of the most massive BH, with the final mass being 10^9–$10^{10} M_{\odot}$ at $z = 0$. It is reported in K15 that only 20% of the total mass of the BH is gained by the merger, of which 75% of the mass is gained below $z = 1$.

The errors on the data points are standard error, calculated as $\sigma/\sqrt{N}$, where σ is the standard deviation and N is the total number of data points in a particular mass bin. We emphasize that the error on the "mean" represents the reliability of the "mean" as a representative number of the binned data. Hence, the standard error on the mean is used to signify the statistical power of the averaging.

The right panel depicts the variation of bolometric luminosity with the host halo mass of BH. The average bolometric luminosity for each halo mass bin is shown in the figure. We note that the luminosities used in this study refer to an instantaneous value. The time-averaged luminosities can also be considered. However, when we consider a statistical sample, we emphasize that the time-averaged luminosity will be equivalent to the average instantaneous luminosity of many black holes (see discussions in Chatterjee et al. 2012). We thus feel confident that the characterization of instantaneous luminosities will be adequate for comparing our theoretical work with observations. We observe that with the increase of the halo mass, the bolometric luminosity of the central AGN increases at both redshifts. But the satellite black hole luminosity is decreasing with the host halo mass. The downsizing observed in the $L_{\rm Bol}$–$M_{\rm halo}$ relation might be a hallmark of the effect of AGN feedback in the simulation. It is likely that the feedback from the central BH is regulating the growth of the satellite BH (see Chatterjee et al. 2012 for discussions).

To further examine Figure 1 we plot the conditional $M_{\rm BH}$–$L_{\rm Bol}$ distributions of central and satellite black holes for two redshifts in Figures 2 and 3. The luminosities represent the average in each black hole mass bin. We note that the luminosity (accretion rate) is almost constant with black hole mass in the lower halo mass bins. Central black hole luminosity is almost constant or increases very slightly with black hole

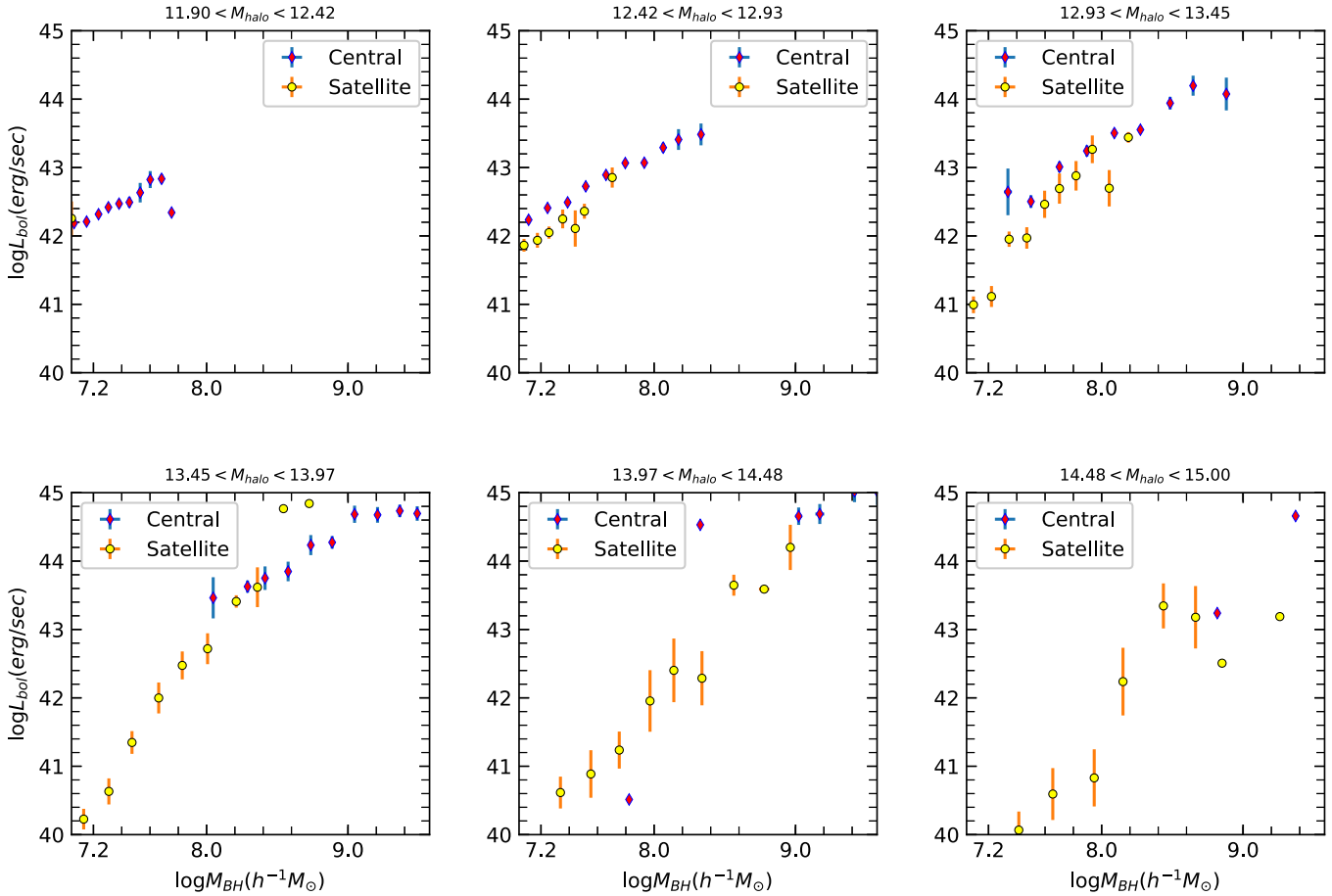

Figure 3. Conditional distribution of the $M_{\rm BH}$–$L_{\rm bol}$ correlations in the simulation at $z = 0.1$. The blue diamonds and yellow circles represent the central and satellite AGNs, respectively. The luminosity of the central AGN slightly increases with $M_{\rm BH}$, while there is a wide spread in the distribution of satellite AGN luminosities with the very low-luminosity AGNs in the high-mass bins. The results are discussed in Sections 3 and 4.

mass in all the halo mass bins at redshift 1.0 and 0.1. At $z = 1.0$ satellite BH luminosity remains unchanged with the BH mass up to a halo mass scale $\approx 10^{13.2} h^{-1} M_{\odot}$. However, above this halo mass range the distribution of luminosities gets wider, while at the highest-mass bin we do see the satellite AGNs with low luminosities. This feature can also be seen at $z = 0.1$. At this redshift the luminosity of the satellite AGN spreads above a halo mass bin of $\approx 10^{12.9} h^{-1} M_{\odot}$. The emergence of lower-luminosity satellite AGNs in higher-mass halos might be a signature of AGN feedback where the supply of cold gas gets cut off due to the additional heating from the central engine.

To explain the result, we show the distribution of the density and temperature of the gas adjacent to the AGN for cases with and without feedback and for two different host halo masses at $z = 1.0$. To differentiate the effect of the halo (gravitational effect) with that of the AGN feedback (non-gravitational effect) on the surrounding diffused gas, we take two black holes at $z = 1$ with identical black hole masses but different host halo masses, and study the density and temperature distribution of their surrounding hot gas. We compute the smoothed temperature and density using the cubic spline kernel.

The results are shown in Figures 4 and 5. Both black holes have a mass $7.7 h^{-1} M_{\odot}$ in logarithmic scale. Both the density and temperature maps in the top right panel are shown for a BH of host halo mass $7.9 \times 10^{13} h^{-1} M_{\odot}$ and the top left panel shows the map around a BH residing in a halo of mass $1.6 \times 10^{12} h^{-1} M_{\odot}$. To understand the effect of feedback, we constructed two more density and temperature maps using no feedback data (bottom panel). The bottom left panels of Figures 4 and 5 show density and temperature maps, respectively, inside a lower-mass halo ($M_{\rm halo} = 1.3 \times 10^{12} h^{-1} M_{\odot}$) and the bottom right panel represents the map inside a higher-mass halo ($M_{\rm halo} = 2.5 \times 10^{13} h^{-1} M_{\odot}$). It is clearly seen from Figures 4 and 5 that the average density and temperature is higher in the higher halo mass in both the cases when AGN feedback is present and absent in the simulation. But the presence of feedback decreases density at the center significantly at both halo mass scales, whereas temperature increases with the feedback. If it were alone the effect of gravitational potential, then we would get the same results for the presence and absence of AGN feedback. It is to be noted that in Figure 5, temperature maps look somewhat grainy. We understand that this is related to the spatial scale of the maps. To investigate this issue further, we have checked the distribution at a larger scale (200 kpc) and found that the maps are smooth, representing the SPH particle field. We also checked the scaling relations at this larger spatial scale, and confirmed that statistically the relations stay the same without altering any of the conclusions.

To study the effect of AGN feedback at $z = 0.1$, we made similar temperature and density maps around two black holes in two different environments—one inside a low-mass halo and another inside a host halo with higher mass. This is shown in Figure 6. Both black holes have very similar masses of $10^{8.2} h^{-1} M_{\odot}$. The left panels show the results for the halo of

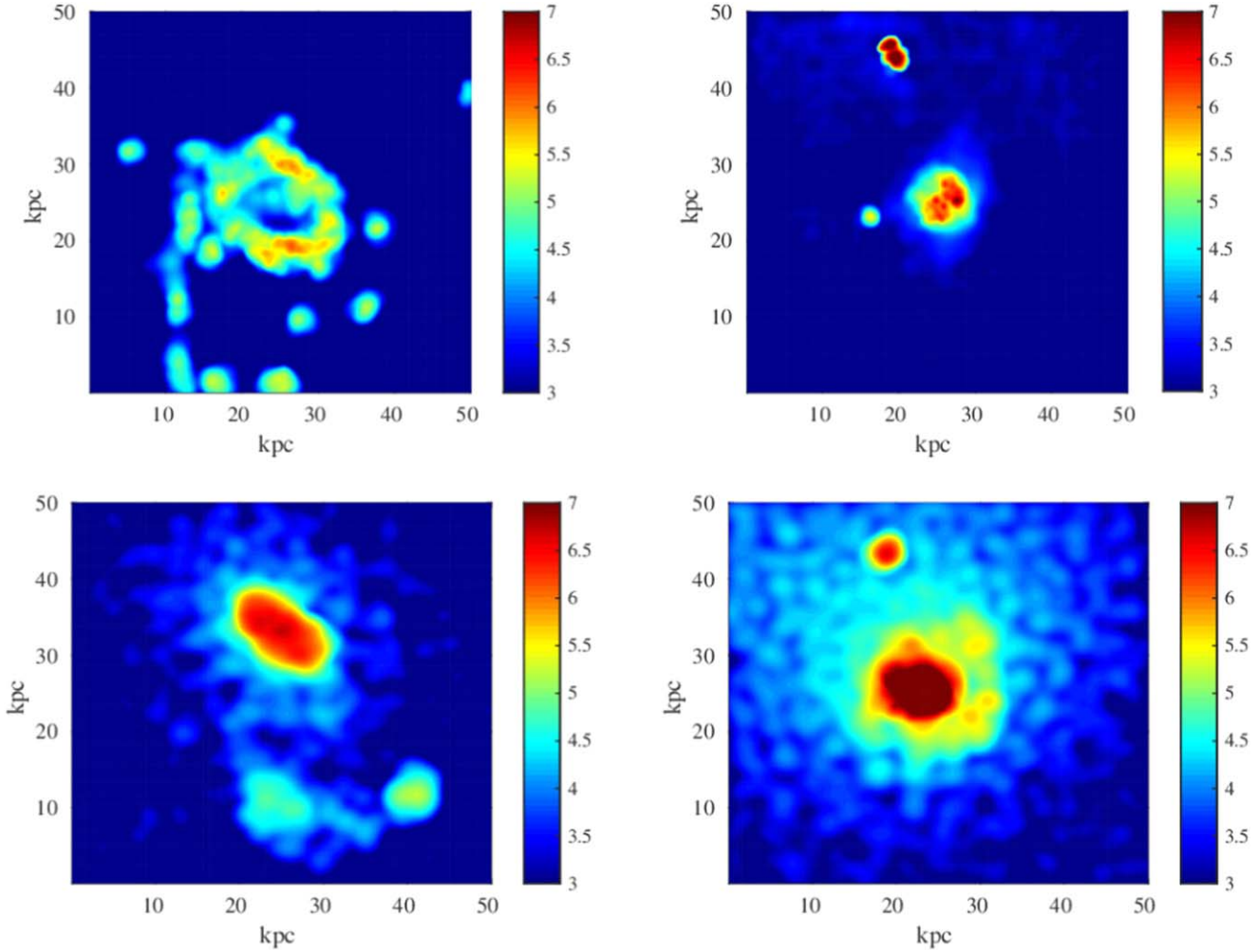

Figure 4. Density map in a region of radius 25 kpc for different physical scenarios. The top panels show the density map for the K15 simulation around two AGNs with similar black hole masses ($\log_{10}(M_{\rm BH}) = 7.7h^{-1}M_{\odot}$), residing in host halos of different masses. The density is shown in units of $M_{\odot}$ kpc^{-3}. The bottom panels show the same maps, except for the cases when AGN feedback is not present in the D08 simulation. Top left panel: density map for the BH hosted by a halo of mass $10^{12.2}h^{-1}M_{\odot}$. Top right panel: density map for a BH residing in a host halo of mass $10^{13.9}h^{-1}M_{\odot}$. It is clearly seen that at higher masses the halo density of gas is high at the center. Bottom left panel: density map inside a halo of mass $10^{12.1}h^{-1}M_{\odot}$. Bottom right panel: density map inside a halo of mass $10^{13.4}h^{-1}M_{\odot}$. In the lower panels too we see a higher density of the diffuse gas for higher-mass halos. However, we can see a clear enhancement of the density when feedback is not present at both halo mass scales. We argue this is due to the effect of AGN feedback, as discussed in Sections 3 and 4.

mass $10^{12.8}h^{-1}M_{\odot}$. The right panels show the results of a halo with a higher mass, $10^{13.8}h^{-1}M_{\odot}$. The top panels show the density distribution inside a region of radius 25 kpc for two AGNs from the K15 simulation in two different halo masses. The temperature distribution of those two AGNs is shown in the bottom panels. We also note that the bolometric luminosities of two AGNs residing at lower- and higher-mass halos are 10^{43} and 10^{44} erg s^{-1}, respectively. The AGN in the lower-mass host halo is more active and this is reflected in the temperature map, where we can see an enhancement of temperature at the center of the bottom left map when compared with the bottom right one. The effect of feedback is also evident in both the density maps, where it is seen that the gas density is lower in the central region of the maps. However, we note that due to the limitations of the D08 and K15 simulations it is not possible to compare the results of $z = 0.1$ with the scenario when feedback is absent. However, we argue that the effects of enhancement of temperature and suppression of density due to feedback effects are ubiquitous at all redshifts.

To check the effect of feedback statistically on the density and temperature of the gas inside the halo, we have obtained the stacked radial profiles of density and temperature in the presence and absence of AGN feedback at $z = 1$. The results are shown in Figure 7. Here the error bars on the data points are the standard errors (as discussed in Section 3) divided by the square root of the total number of stacked maps, in order to take into account the stacking error. The left panel of this figure shows the radial profile of the stacked density inside the 25 kpc radius region. The blue diamonds represent the D08 "without feedback" density profile, while the red dot shows the density profile for the K15 simulation. We can see a decrement of gas density at the central region in the presence of AGN feedback, supporting our claim that feedback energy drives the hot gas outward, creating the underdense region surrounding the AGN. Slight enhancement of density in the presence of feedback is seen at radii >10 kpc, although this is within the error bar. However, we explain that this overdensity is probably coming from the accumulation of gas that has been pushed out of the central region due to feedback. A similar feature is also found in the radial profile of the X-ray flux (Mukherjee et al. 2019), as the main X-ray-emitting mechanism from clusters is thermal bremsstrahlung. Thus, it is expected that the density profile will

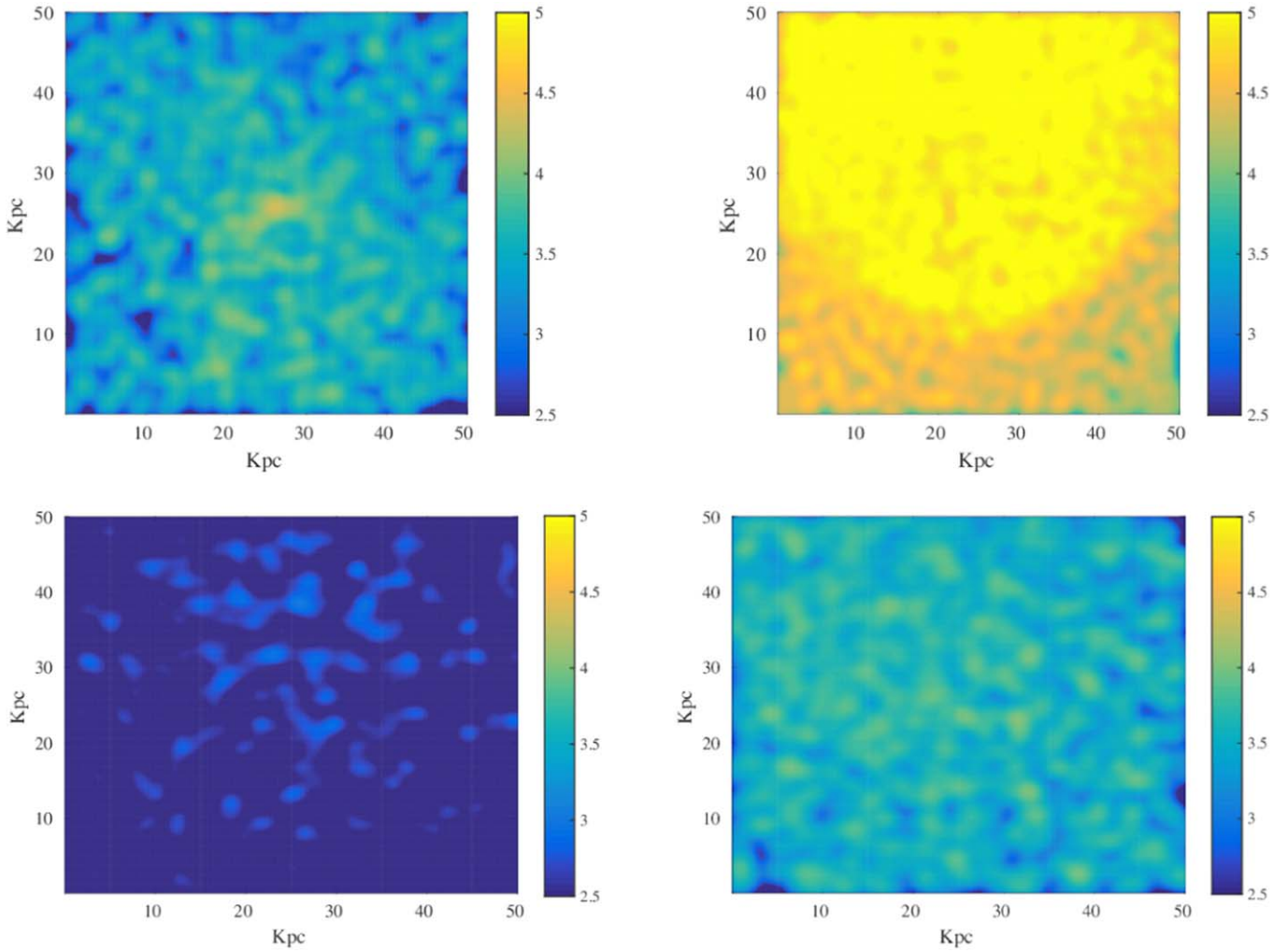

Figure 5. Temperature map in a region of radius 25 kpc for different physical scenarios. The top panels show the temperature maps for the K15 simulation around two AGNs with similar black hole mass ($\log_{10}(M_{\rm BH}) = 7.7h^{-1}M_{\odot}$), residing in host halos of different masses. The temperature is in Kelvin. The bottom panels show the same maps, except for the case when AGN feedback is not present in the case of a D08 simulation. Top left panel: temperature map of the diffuse gas around the BH hosted by a halo of mass $10^{12.2}h^{-1}M_{\odot}$. Top right panel: temperature map of the surrounding gas of a BH residing in a host halo of mass $10^{13.9}h^{-1}M_{\odot}$. It is clear that at higher masses halo temperature is high at the center. Bottom left panel: temperature map inside a halo of mass $10^{12.1}h^{-1}M_{\odot}$. Bottom right panel: temperature map inside a halo of mass $10^{13.4}h^{-1}M_{\odot}$. In the lower panels too we see higher temperatures for higher-mass halos. However, we can see a clear enhancement of temperature when feedback is present at both halo mass scales. We argue that this is due to the effect of AGN feedback, as discussed in Sections 3 and 4.

follow the X-ray profile. The right panel of Figure 7 represents the stacked temperature profile. The blue diamonds and red dots show the stacked temperature for the D08 simulation "without feedback" and the K15 simulation, respectively. The clear enhancement of temperature in the presence of AGN feedback is in accordance with our claim that the gas surrounding AGNs is heated by the feedback energy.

Finally, to check the effect of AGN feedback from a different perspective, we plot the stellar mass with the corresponding halo mass. We define stellar mass as the total mass of the stars inside a radius which is equal to $0.2R_{200}$. R_{200} is the usual radius where the density of the halo becomes 200 times the critical density. This is shown in Figure 8. Here, blue diamonds represent the case when AGN feedback is absent in the D08 simulation at $z = 1.0$. The red stars and green triangles are for K15 simulation at $z = 1.0$ and $z = 0.1$, respectively. It is clearly seen from the figure that the presence of feedback reduces the stellar mass when compared with the case of "without feedback." Also, it is seen that the stellar mass is higher at $z = 0.1$ compared to $z = 1.0$. Here, we note that the definition of stellar mass used in this paper may be different from the other groups. For example, Khandai et al. (2015) define galaxies as the subhalos consisting of more than 100 dark matter particles, and their stellar mass is represented by the mass of the subhalos. In Torrey et al. (2014) stellar mass is defined as the total mass of the stars within twice the half-mass–radius. We wish to carefully note this difference and emphasize the fact that feedback from an AGN shuts down star formation in its vicinity by limiting the availability of cold gas.

4. Discussion

In this work we study the global role of AGN feedback on the accretion of the AGN itself, as well as its impact on large-scale environments of AGN, using a cosmological volume simulation. In the left panel of Figure 1 we observe a strong correlation between the mass of the central SMBH with their host dark matter halos, consistent with other observation and simulation results (e.g., Ferrarese 2002; Baes et al. 2003; Colberg & Di Matteo 2008; Booth & Schaye 2010; Filloux et al. 2010;

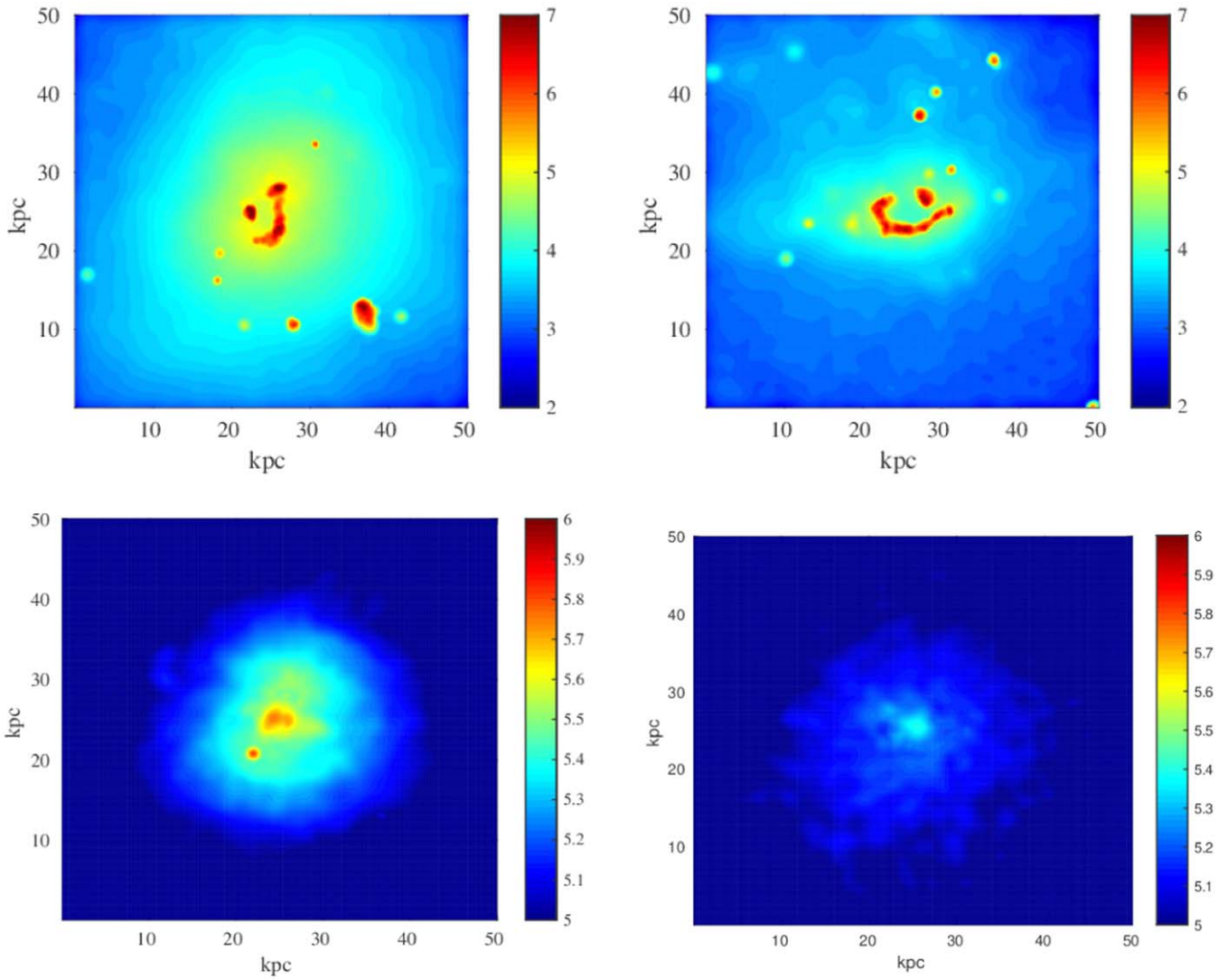

Figure 6. Density and temperature maps in a region of radius 25 kpc around two AGNs of similar mass in different halo environments at $z = 0.1$. The top panels show the density maps for the K15 simulation around two AGNs with similar black hole masses ($\log_{10}(M_{\rm BH}) = 8.2h^{-1}M_{\odot}$), residing in host halos of different masses. The density is shown in units of $M_{\odot}$ kpc^{-3}. The bottom panels shows temperature maps for a similar situation. The color bar shows the temperature in Kelvin. Top left panel: density map of the diffuse gas around the BH hosted by a halo of mass $10^{12.8}h^{-1}M_{\odot}$. Top right panel: density map of the surrounding gas of a BH residing in a host halo of mass $10^{13.8}h^{-1}M_{\odot}$. Bottom left panel: temperature map inside a halo of mass $10^{12.8}h^{-1}M_{\odot}$. Bottom right panel: temperature map inside a halo of mass $10^{13.8}h^{-1}M_{\odot}$. The effect of AGN feedback can be clearly seen from the density maps.

Khandai et al. 2015; Sabra et al. 2015). We see that at both redshifts 1.0 and 0.1, central BH mass is increasing with host halo mass, while the satellite BH mass is increasing weakly while saturating at the higher-mass end. However, no redshift evolution of this correlation is observed.

The right panel of Figure 1 shows a downsizing of satellite AGN luminosity with halo mass at $z = 1.0$ and $z = 0.1$, a result that has been observed in clustering studies of AGNs (e.g., Richardson et al. 2012, 2013). However, the bolometric luminosities of the central AGN increase with the host halo mass. It is possible that the accretion and feedback from the central AGN affect the evolution of the satellites. Chatterjee et al. (2012) tried to investigate the effect of feedback from the central AGN on the satellite AGN but they did not find any significant effect. But we note that the studies of Chatterjee et al. (2012) were confined to halo mass scales of $10^{13}M_{\odot}$. Our results do not exhibit a substantial difference until a mass scale of $10^{13}M_{\odot}$, but we find that the effect becomes significant above this halo mass scale. Richardson et al. (2013) showed that bright optically selected quasars with higher bolometric luminosities reside in lower-mass halos compared to X-ray AGNs with less luminosity. Some authors claim that the depletion of cold gas inside higher-mass halos due to shock heating is responsible for shutting down black hole accretion (e.g., Sijacki et al. 2007; Di Matteo et al. 2012; Gaspari et al. 2013). Another possibility that exists in the literature is "AGN feedback." In this study we addressed this question by looking at the density and temperature of the gas in the vicinity of the black hole.

In a given cluster/galaxy we can consider two effects: gas falling into the gravitational potential well of the cluster gets heated, and the central SMBH displacing the gas via mechanical or radiative feedback. If the effect of halo dominates over feedback then an increase in the density of the diffuse gas is expected in the central region of the halo and BH mass will be correlated with halo mass. But these correlations can get altered if additional heating or cooling mechanisms are present. In Figure 1 we observe a downsizing

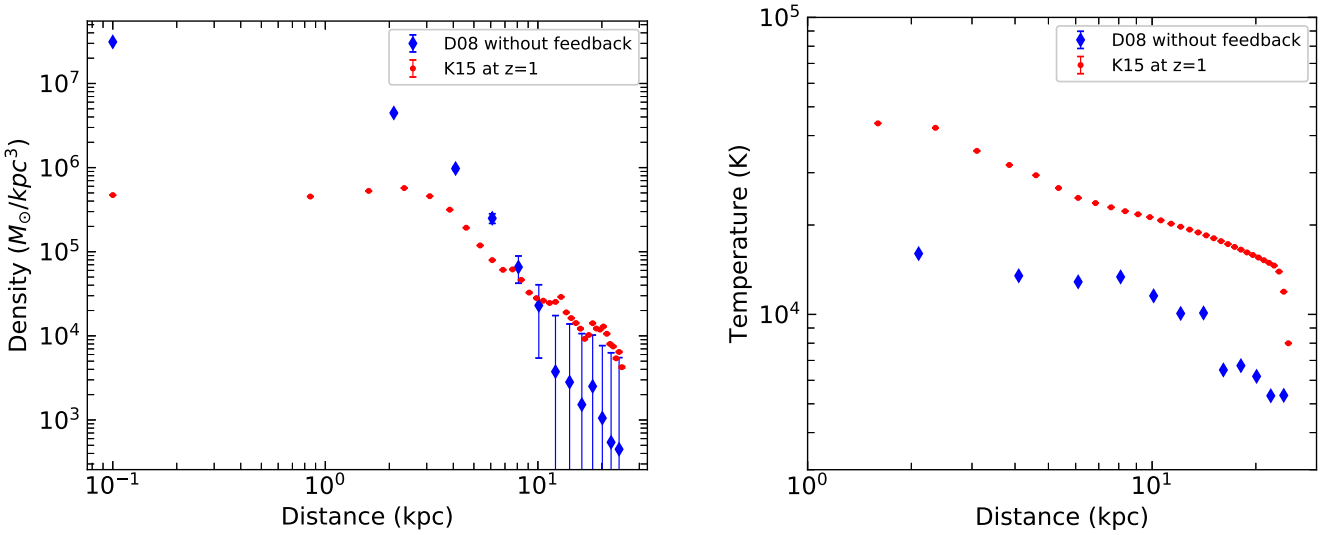

Figure 7. Left panel: radial profile of the stacked density in the presence and absence of AGN feedback inside a region of radius 25 kpc at $z = 1$. The blue diamond represents the density profile when AGN feedback is absent in D08. The red dot shows the scenario when AGN feedback is present in K15. A significant reduction of density at the central region in the presence of AGN feedback supports our claim of displacement of hot gas as a result of AGN feedback. Right panel: stacked radial profile of the temperature in the presence and absence of AGN feedback inside a region of radius 25 kpc at $z = 1$. The blue diamond signs are representative of the temperature profile when AGN feedback is absent in D08. The red dots exhibit that condition when AGN feedback is present in K15. The error bars on the data points in both the panels are the standard errors (as discussed in Section 3) divided by the square root of the number of stacked maps to include the stacking error. A clear enhancement of temperature at the central region in the presence of AGN feedback supports our claim of heating the surrounding gas as a result of AGN feedback. See Sections 3 and 4 for more discussions.

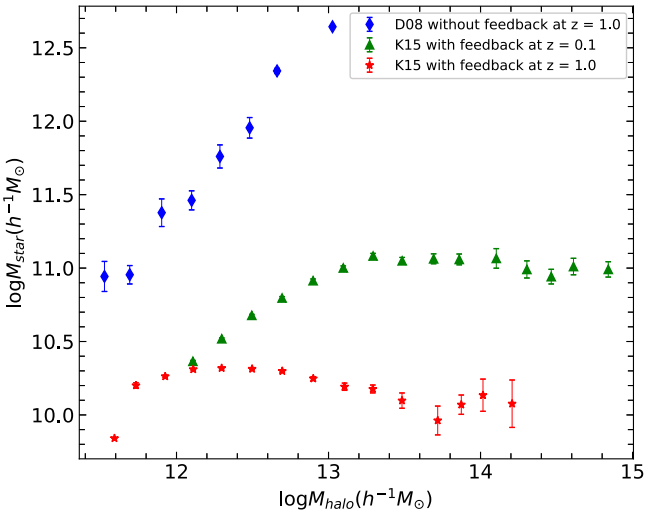

Figure 8. Variation of stellar mass (see definition of stellar mass in Section 2) with the corresponding halo mass bin. The blue diamonds represent the case when AGN feedback is absent in the D08 simulation at $z = 1$. The red stars and green triangles are representative of the K15 simulation at $z = 1$ and $z = 0.1$, respectively. A clear deficit of stellar mass is seen in the presence of AGN feedback in the same halo mass bin when compared with the simulation where AGN feedback is absent. The results are discussed in Sections 3 and 4.

of the BH luminosity. We argue that the feedback effect from AGN is at play here. The outflow from the AGN will displace the hot gas outward, thereby reducing the average density. Thus, the supply of cold gas gets cut inside the higher-mass halo, which results in the suppression of the BH mass. Another possibility for this effect would be the shock heating inside the halo itself.

To disentangle the effect of feedback and halo potential on the diffuse gas, we compute the density and temperature maps around two equally massive BHs (Figures 4 and 5, respectively) and compared them with the scenario when feedback is absent (respectively the bottom panels of Figures 4 and 5). In Figure 4, left panels are density maps around AGNs residing at higher-mass halos and right panels are density maps of diffused gas around AGNs at lower-mass halos. We clearly see an excess of the density in the left panels, which represent higher-mass halos in both cases. However, when we compare the "with feedback" case with the "no feedback" case, we observe a deficit in density at both halo masses.

In Figure 5 we compute the average smoothed temperature of the gas in the central region of the halo for all four cases and we find that with the presence of AGN feedback the temperature of the gas is higher at both halo mass scales, as has been reported previously by Chatterjee et al. (2008). We thus propose that AGN feedback is a significant mechanism for heating and depletion of the cold gas inside the higher-mass halos, thus resulting in the observed downsizing in Figure 1 (AGN luminosity with halo mass). This result is also supported by Figures 2 and 3, where we have plotted the variation of bolometric luminosity of central and satellite AGNs with their masses at different host halo mass bins at $z = 1$ and $z = 0.1$, respectively. We see a spread in the bolometric luminosity of satellite AGNs in the higher-mass host halo bins with very low-luminosity AGNs.

In Figure 6, we examine the effects of AGNs and the host halo potential on the hot gas at $z = 0.1$. From the density map the signature of AGN feedback is evident at the central region where the gas is pushed outward, resulting in a deficit in the density map. However, from the temperature map, we can see that the temperature of the gas is higher at the low halo mass. Here, we note that the bolometric luminosity of the BH inside the low-mass halo is higher. Hence, we can conclude that the more active AGN energizes its surrounding medium more, causing an enhancement of temperature.

Finally, in Figure 7, we investigate the effect of AGN feedback on the density and temperature of the gas statistically

by computing their stacked profile. It is evident from this figure that the density of the gas decreases statistically in the presence of AGN feedback. Moreover, the right panel of the figure shows that the presence of AGN feedback is enhancing the temperature of the central region of the halo statistically. The overall enhancement of temperature and decrement of density of the gas inside the halo supports our claim of feedback activity. In addition to temperature and density we study the correlation between their stellar mass with the corresponding halo mass in the presence and absence of AGN feedback (Figure 8). In this figure, we see that the stellar mass is significantly low in the presence of AGN feedback when compared with the case with an absence of feedback. We can explain that AGN feedback heats the surrounding gas so significantly that the availability of cold gas gets depleted thereby reducing the stellar mass.

In recent studies involving X-ray stacking analyses of AGNs at moderately high redshift ($z \approx 0.6$) Chatterjee et al. (2015) and Mukherjee et al. (2019) showed that AGNs at large have lower X-ray fluxes in the central region compared to the X-ray flux of galaxies without AGNs. They propose a promising technique for studying the X-ray gas in higher-redshift galaxies for quantifying AGN feedback. In this work we study the effect of AGN feedback on temperature, density, and stellar mass and examine their global effects. In a follow-up paper, using K15 and D08 data (Kar Chowdhury et al. 2019, in preparation) we perform a detailed X-ray analysis of the ICM and compare our results with the studies of Chatterjee et al. (2015) and Mukherjee et al. (2019).

Finally, we note that the simulation used for this work has several limitations. The accretion onto the BH is based on a simplistic spherical accretion model. The spatial resolution of the simulation is limited to all the precise relativistic accretion flow in the simulation. Furthermore, the energy due to feedback from the black hole is assumed to be distributed isotropically among the gas particles surrounding them in a region within the smoothing length. Momentum-driven outflow from the AGN has not been taken into account in the simulation. But we note that as the effects of BH accretion on the resolved large-scale environment match with the observations, Bondi model can be used to study the effect of AGN on the cosmological scale (Di Matteo et al. 2008). Also, it has been carefully noted that the effect of linking the black hole with its surrounding medium is independent of the coupling model as long as the coupling scale and time are small compared to the scale and dynamical time of the host galaxy (Di Matteo et al. 2008).

A plethora of work has been done by different groups to understand the growth of AGN and its effect on the surrounding medium using cosmological simulation and correlate the results with different observables. Le Brun et al. (2014) ran cosmological hydrodynamic simulation cosmo-OWLS to examine different scaling relations between various properties of galaxy groups and clusters and compared it to observations. They found that the density profile is lower at the central region in the presence of strong AGN feedback activity, which agrees well with our result (left panel of Figure 7). Also, the $M_{\rm BH}$–$M_{\rm halo}$ relation obtained by them qualitatively agrees with our finding. In another recent work Le Brun et al. (2017) make use of cosmo-OWLS simulation (Le Brun et al. 2014; McCarthy et al. 2014) to explore the scatter and evolution of the scaling relations between the properties of the hot gas inside galaxy clusters. Their result for the evolution of the scaling relation between halo mass and bolometric luminosity agrees well with our result. Rosas-Guevara et al. (2016) investigated different observable properties of SMBH to study their evolution from an early time to the current epoch using the EAGLE simulation (Crain et al. 2015; Schaye et al. 2015). In this paper the authors have reported a rapid growth of black hole mass in the halo mass range $10^{11.5}$–$10^{12.5} M_{\odot}$. This active growth continues until the BH reaches $10^{8} M_{\odot}$. Also, in the higher-mass halo BH grows linearly. We do not see such a trend mainly because we limit our sample with a BH mass well above the seed mass and also for halo mass $>10^{12} M_{\odot}$. However, they found very little redshift evolution of this scaling relation, which is consistent with our results. Barnes et al. (2017) studied the global properties of galaxy clusters as well as the profiles of the hot gas inside them. They also studied X-ray and SZ properties of the hot gas inside the clusters and matched them with observations. They have used the Cluster-EAGLE simulation project, which is a collection of zoom simulations of formation of thirty galaxy clusters. Their density and temperature profiles showing less dense and hotter temperature of the gas at the central region again is in accordance with our claim of AGN feedback activity.

Our study conclusively establishes the effect of AGN feedback and its implication on diffuse gas in galaxy groups and clusters and corroborates several previous other observational and theoretical work. Although the conclusion is robust, we would like to stress that it might be sensitive to the particular sub-grid model of AGN feedback that is used in this simulation. Hence, comparison with observational results is absolutely essential to establish the fidelity of our studies. Starting from the effect of AGN feedback on its surrounding hot gas, we study the evolution of AGNs with their host halos. We elaborate new observations to verify the claims presented in our work and propose conducting a detailed comparison between observed and simulated data in the future.

We thank the referee for some very important comments that helped improve the draft. S.C. acknowledges financial support from the Department of Science and Technology through the SERB Early Career Research grant and Presidency University through the Faculty Research and Professional Development Funds. S.C. is grateful to the Inter University Center for Astronomy and Astrophysics (IUCAA) for providing infrastructural and financial support, along with local hospitality through the IUCAA-associateship program. R.K.C. acknowledges the Department of Science and Technology for the INSPIRE fellowship. R.K.C. is grateful to IUCAA, Dr. Saumyadip Samui, and Dr. Ritaban Chatterjee for computational support. R.K.C. thanks Alankar Dutta for his codes used in reading the snapfiles of the K15 simulation. R.K.C. and S.C. thank Andrea Lapi, Sowgat Muzahid, and members of the PRESIPACT research group for useful discussions about this work.

N.K. is supported by the Ramanujan Fellowship awarded by the Department of Science and Technology, Government of India. The simulations were run on the Cray XT5 supercomputer Kraken at the National Institute for Computational Sciences. The analysis was partially done on the xanadu cluster funded by the Ramanujan Fellowship at NISER. N.K. and T.D.M. acknowledge support from the National Science Foundation (NSF) PetaApps program, OCI-0749212 and by NSF AST-1009781.

ORCID iDs

Suchetana Chatterjee https://orcid.org/0000-0002-3236-2853

References

Aller, M. C., & Richstone, D. O. 2007, ApJ, 665, 120
Arnaud, M., & Evrard, A. E. 1999, MNRAS, 305, 631
Aversa, R., Lapi, A., de Zotti, G., Shankar, F., & Danese, L. 2015, ApJ, 810, 74
Baes, M., Buyle, P., Hau, G. K. T., & Dejonghe, H. 2003, MNRAS, 341, L44
Barai, P., Viel, M., Murante, G., Gaspari, M., & Borgani, S. 2014, MNRAS, 437, 1456
Barnes, D. J., Kay, S. T., Bahé, Y. M., et al. 2017, MNRAS, 471, 1088
Baron, D., Netzer, H., Poznanski, D., Prochaska, J. X., & Förster Schreiber, N. M. 2017, MNRAS, 470, 1687
Battaglia, N., Bond, J. R., Pfrommer, C., Sievers, J. L., & Sijacki, D. 2010, ApJ, 725, 91
Beckmann, R. S., Devriendt, J., Slyz, A., et al. 2017, MNRAS, 472, 949
Beifiori, A., Courteau, S., Corsini, E. M., & Zhu, Y. 2012, MNRAS, 419, 2497
Bharadwaj, V., Reiprich, T. H., Lovisari, L., & Eckmiller, H. J. 2015, A&A, 573, A75
Bhattacharya, S., Di Matteo, T., & Kosowsky, A. 2008, MNRAS, 389, 34
Biernacki, P., Teyssier, R., & Bleuler, A. 2017, MNRAS, 469, 295
Bondi, H. 1952, MNRAS, 112, 195
Bondi, H., & Hoyle, F. 1944, MNRAS, 104, 273
Booth, C. M., & Schaye, J. 2009, MNRAS, 398, 53
Booth, C. M., & Schaye, J. 2010, MNRAS, 405, L1
Caplar, N., Lilly, S. J., & Trakhtenbrot, B. 2015, ApJ, 811, 148
Cattaneo, A., Dekel, A., Devriendt, J., Guiderdoni, B., & Blaizot, J. 2006, MNRAS, 370, 1651
Cattaneo, A., & Teyssier, R. 2007, MNRAS, 376, 1547
Chatterjee, S., Degraf, C., Richardson, J., et al. 2012, MNRAS, 419, 2657
Chatterjee, S., Di Matteo, T., Kosowsky, A., & Pelupessy, I. 2008, MNRAS, 390, 535
Chatterjee, S., Ho, S., Newman, J. A., & Kosowsky, A. 2010, ApJ, 720, 299
Chatterjee, S., & Kosowsky, A. 2007, ApJL, 661, L113
Chatterjee, S., Newman, J. A., Jeltema, T., et al. 2015, PASP, 127, 716
Chaudhuri, A., Majumdar, S., & Nath, B. B. 2013, ApJ, 776, 84
Choi, E., Ostriker, J. P., Naab, T., Oser, L., & Moster, B. P. 2015, MNRAS, 449, 4105
Cielo, S., Bieri, R., Volonteri, M., Wagner, A. Y., & Dubois, Y. 2018, MNRAS, 477, 1336
Ciotti, L., & Ostriker, J. P. 2001, ApJ, 551, 131
Colberg, J. M., & Di Matteo, T. 2008, MNRAS, 387, 1163
Conroy, C., & White, M. 2013, ApJ, 762, 70
Costa, T., Sijacki, D., & Haehnelt, M. G. 2015, MNRAS, 448, L30
Cox, T. J., Dutta, S. N., Di Matteo, T., et al. 2006, ApJ, 650, 791
Crain, R. A., Schaye, J., Bower, R. G., et al. 2015, MNRAS, 450, 1937
Crichton, D., Gralla, M. B., Hall, K., et al. 2016, MNRAS, 458, 1478
Croton, D. J., Springel, V., White, S. D. M., et al. 2006, MNRAS, 365, 11
Davis, M., Efstathiou, G., Frenk, C. S., & White, S. D. M. 1985, ApJ, 292, 371
Di Matteo, T., Colberg, J., Springel, V., Hernquist, L., & Sijacki, D. 2008, ApJ, 676, 33
Di Matteo, T., Khandai, N., DeGraf, C., et al. 2012, ApJL, 745, L29
Di Matteo, T., Springel, V., & Hernquist, L. 2005, Natur, 433, 604
Dressler, A. 1989, in IAU Symp. 134, Active Galactic Nuclei, ed. D. E. Osterbrock & J. S. Miller (Dordrecht: Kluwer), 217
Feoli, A., & Mancini, L. 2009, ApJ, 703, 1502
Ferrarese, L. 2002, ApJ, 578, 90
Ferrarese, L., Côté, P., Dalla Bontà, E., et al. 2006, ApJL, 644, L21
Ferrarese, L., & Ford, H. 2005, SSRv, 116, 523
Ferrarese, L., & Merritt, D. 2000, ApJL, 539, L9
Filloux, C., Durier, F., Pacheco, J. A. F., & Silk, J. 2010, IJMPD, 19, 1233
Gaspari, M., Brighenti, F., & Ruszkowski, M. 2013, AN, 334, 394
Gaspari, M., Brighenti, F., & Temi, P. 2012, MNRAS, 424, 190
Genel, S., Vogelsberger, M., Springel, V., et al. 2014, MNRAS, 445, 175
Graham, A. W. 2007, MNRAS, 379, 711
Graham, A. W., & Driver, S. P. 2007, ApJ, 655, 77
Granato, G. L., De Zotti, G., Silva, L., Bressan, A., & Danese, L. 2004, ApJ, 600, 580
Gültekin, K., Richstone, D. O., Gebhardt, K., et al. 2009, ApJ, 698, 198
Hambrick, D. C., Ostriker, J. P., Naab, T., & Johansson, P. H. 2011, ApJ, 738, 16
Häring, N., & Rix, H.-W. 2004, ApJL, 604, L89
Harrison, C. M., Costa, T., Tadhunter, C. N., et al. 2018, NatAs, 2, 198
Heckman, T. M., & Best, P. N. 2014, ARA&A, 52, 589
Hirschmann, M., Dolag, K., Saro, A., et al. 2014, MNRAS, 442, 2304
Hopkins, P. F., Hernquist, L., Cox, T. J., et al. 2006a, ApJS, 163, 1
Hopkins, P. F., Hernquist, L., Cox, T. J., Robertson, B., & Krause, E. 2007a, ApJ, 669, 45
Hopkins, P. F., Hernquist, L., Cox, T. J., Robertson, B., & Krause, E. 2007b, ApJ, 669, 67
Hopkins, P. F., Robertson, B., Krause, E., Hernquist, L., & Cox, T. J. 2006b, ApJ, 652, 107
Johansson, P. H., Burkert, A., & Naab, T. 2009, ApJL, 707, L184
Kaiser, C. R., & Binney, J. 2003, MNRAS, 338, 837
Kakkad, D., Mainieri, V., Brusa, M., et al. 2017, MNRAS, 468, 4205
Katz, N., Weinberg, D. H., & Hernquist, L. 1996, ApJS, 105, 19
Kauffmann, G., & Haehnelt, M. 2000, MNRAS, 311, 576
Kauffmann, G., Heckman, T. M., Tremonti, C., et al. 2003, MNRAS, 346, 1055
Khandai, N., Di Matteo, T., Croft, R., et al. 2015, MNRAS, 450, 1349
Komatsu, E., Smith, K. M., Dunkley, J., et al. 2011, ApJS, 192, 18
Kormendy, J., & Richstone, D. 1995, ARA&A, 33, 581
Lacy, M., Mason, B., Sarazin, C., et al. 2019, MNRAS, 483, L22
Lanzuisi, G., Delvecchio, I., Berta, S., et al. 2017, A&A, 602, A123
Lapi, A., Cavaliere, A., & Menci, N. 2005, ApJ, 619, 60
Lapi, A., Raimundo, S., Aversa, R., et al. 2014, ApJ, 782, 69
Lapi, A., Shankar, F., Mao, J., et al. 2006, ApJ, 650, 42
Le Brun, A. M. C., McCarthy, I. G., Schaye, J., & Ponman, T. J. 2014, MNRAS, 441, 1270
Le Brun, A. M. C., McCarthy, I. G., Schaye, J., & Ponman, T. J. 2017, MNRAS, 466, 4442
Li, Y., Bryan, G. L., Ruszkowski, M., et al. 2015, ApJ, 811, 73
Li, Y., Hernquist, L., Robertson, B., et al. 2007, ApJ, 665, 187
Liu, M., Di Matteo, T., & Feng, Y. 2016, MNRAS, 458, 1402
Lu, Z., & Mo, H. J. 2015, ApJ, 802, 110
Magorrian, J., Tremaine, S., Richstone, D., et al. 1998, AJ, 115, 2285
Marconi, A., & Hunt, L. K. 2003, ApJL, 589, L21
Marconi, A., Risaliti, G., Gilli, R., et al. 2004, MNRAS, 351, 169
McCarthy, I. G., Le Brun, A. M. C., Schaye, J., & Holder, G. P. 2014, MNRAS, 440, 3645
McCarthy, I. G., Schaye, J., Ponman, T. J., et al. 2010, MNRAS, 406, 822
Merritt, D., & Ferrarese, L. 2001, ApJ, 547, 140
Monaco, P., Fontanot, F., & Taffoni, G. 2007, MNRAS, 375, 1189
Monaghan, J. J. 1992, ARA&A, 30, 543
Mukherjee, S., Bhattacharjee, A., Chatterjee, S., Newman, J. A., & Yan, R. 2019, ApJ, 872, 35
Mutlu-Pakdil, B., Seigar, M. S., Hewitt, I. B., et al. 2018, MNRAS, 474, 2594
Nath, B. B., & Roychowdhury, S. 2002, MNRAS, 333, 145
Nelson, D., Genel, S., Vogelsberger, M., et al. 2015, MNRAS, 448, 59
Nulsen, P., McNamara, B., David, L., & Wise, M. 2004, 35th COSPAR Seientific Assembly, ed. J.-P. Paillé, (Paris), 3235
Oogi, T., Enoki, M., Ishiyama, T., et al. 2016, MNRAS, 456, L30
Peirani, S., Sonnenfeld, A., Gavazzi, R., et al. 2019, MNRAS, 483, 4615
Pelupessy, F. I., Di Matteo, T., & Ciardi, B. 2007, ApJ, 665, 107
Penny, S. J., Masters, K. L., Smethurst, R., et al. 2018, MNRAS, 476, 979
Peterson, J. R., & Fabian, A. C. 2006, PhR, 427, 1
Puchwein, E., Springel, V., Sijacki, D., & Dolag, K. 2010, MNRAS, 406, 936
Raychaudhury, S., Giacintucci, S., O'Sullivan, E., et al. 2009, in ASP Conf. Ser. 407, The Low-Frequency Radio Universe, ed. D. J. Saikia et al. (San Francisco, CA: ASP), 246
Richardson, J., Chatterjee, S., Zheng, Z., Myers, A. D., & Hickox, R. 2013, ApJ, 774, 143
Richardson, J., Zheng, Z., Chatterjee, S., Nagai, D., & Shen, Y. 2012, ApJ, 755, 30
Rosas-Guevara, Y., Bower, R. G., Schaye, J., et al. 2016, MNRAS, 462, 190
Ruan, J. J., McQuinn, M., & Anderson, S. F. 2015, ApJ, 802, 135
Sabra, B. M., Saliba, C., Abi Akl, M., & Chahine, G. 2015, ApJ, 803, 5
Saikia, P., Körding, E., & Falcke, H. 2015, MNRAS, 450, 2317
Scannapieco, E., & Oh, S. P. 2004, ApJ, 608, 62
Scannapieco, E., Thacker, R. J., & Couchman, H. M. P. 2008, ApJ, 678, 674
Schaye, J., Crain, R. A., Bower, R. G., et al. 2015, MNRAS, 446, 521
Scholtz, J., Alexander, D. M., Harrison, C. M., et al. 2018, MNRAS, 475, 1288
Shakura, N. I., & Sunyaev, R. A. 1973, A&A, 24, 337
Shankar, F., Salucci, P., Granato, G. L., De Zotti, G., & Danese, L. 2004, MNRAS, 354, 1020
Sijacki, D., Springel, V., Di Matteo, T., & Hernquist, L. 2007, MNRAS, 380, 877
Sijacki, D., Vogelsberger, M., Genel, S., et al. 2015, MNRAS, 452, 575

Silk, J., & Rees, M. J. 1998, A&A, 331, L1
Soltan, A. 1982, MNRAS, 200, 115
Spacek, A., Scannapieco, E., Cohen, S., Joshi, B., & Mauskopf, P. 2016, ApJ, 819, 128
Spergel, D. N., Verde, L., Peiris, H. V., et al. 2003, ApJS, 148, 175
Springel, V. 2005, MNRAS, 364, 1105
Springel, V., Di Matteo, T., & Hernquist, L. 2005, MNRAS, 361, 776
Springel, V., & Hernquist, L. 2003, MNRAS, 339, 312
Springel, V., White, S. D. M., Tormen, G., & Kauffmann, G. 2001, MNRAS, 328, 726
Steinborn, L. K., Dolag, K., Hirschmann, M., Prieto, M. A., & Remus, R.-S. 2015, MNRAS, 448, 1504
Sunyaev, R. A., & Zeldovich, Y. B. 1972, CoASP, 4, 173
Terrazas, B. A., Bell, E. F., Woo, J., & Henriques, B. M. B. 2017, ApJ, 844, 170
Teyssier, R. 2002, A&A, 385, 337
Teyssier, R., Moore, B., Martizzi, D., Dubois, Y., & Mayer, L. 2011, MNRAS, 414, 195
Thacker, R. J., Scannapieco, E., Couchman, H. M. P., & Richardson, M. 2009, ApJ, 693, 552
Torrey, P., Vogelsberger, M., Genel, S., et al. 2014, MNRAS, 438, 1985
Tremaine, S., Gebhardt, K., Bender, R., et al. 2002, ApJ, 574, 740
Vaddi, S., O'Dea, C. P., Baum, S. A., et al. 2016, ApJ, 818, 182
van den Bosch, R. C. E. 2016, ApJ, 831, 134
Vazza, F., Brüggen, M., & Gheller, C. 2013, MNRAS, 428, 2366
Verdier, L., Melin, J.-B., Bartlett, J. G., et al. 2016, A&A, 588, A61
Vitale, M., Mignoli, M., Cimatti, A., et al. 2013, A&A, 556, A11
Vittorini, V., Shankar, F., & Cavaliere, A. 2005, MNRAS, 363, 1376
Vogelsberger, M., Genel, S., Springel, V., et al. 2014a, MNRAS, 444, 1518
Vogelsberger, M., Genel, S., Springel, V., et al. 2014b, Natur, 509, 177
Voit, G. M., Ma, C. P., Greene, J., et al. 2018, ApJ, 853, 78
Volonteri, M., Natarajan, P., & Gültekin, K. 2011, ApJ, 737, 50
Wyithe, J. S. B., & Loeb, A. 2003, ApJ, 595, 614
Yang, G., Brandt, W. N., Vito, F., et al. 2018, MNRAS, 475, 1887
Zanni, C., Murante, G., Bodo, G., et al. 2005, A&A, 429, 399